Editors' Suggestion

Giant Bulk Electrophotovoltaic Effect in Heteronodal-Line Systems

Xiao Jiang,[1] Lei Kang,[2] Jianfeng Wang,[3] and Bing Huang[1,4,*]
[1]Beijing Computational Science Research Center, Beijing 100193, China
[2]Technical Institute of Physics and Chemistry, Chinese Academy of Sciences, Beijing 100190, China
[3]School of Physics, Beihang University, Beijing 100191, China
[4]Beijing Normal University, Beijing 100875, China

(Received 17 November 2022; revised 27 April 2023; accepted 30 May 2023; published 22 June 2023)

The realization of a giant and continuously tunable second-order photocurrent is desired for many nonlinear optical (NLO) and optoelectronic applications, which remains a great challenge. Here, based on a two-band model, we propose a concept of the bulk electrophotovoltaic effect, that is, an out-of-plane external electric field (E_{ext}) that can continuously tune in-plane shift current along with its sign flip in a heteronodal-line (HNL) system. While strong linear optical transition around the nodal loop may potentially generate giant shift current, an E_{ext} can effectively control the radius of the nodal loop, which can continuously modulate the shift-vector components inside and outside the nodal loop holding opposite signs. This concept has been demonstrated in the HNL $HSnN/MoS_2$ system using first-principles calculations. The $HSnN/MoS_2$ heterobilayer can not only produce a shift-current conductivity with magnitude that is one to two orders larger than other reported systems, but it can also realize a giant bulk electrophotovoltaic effect. Our finding opens new routes to create and manipulate NLO responses in 2D materials.

DOI: 10.1103/PhysRevLett.130.256902

Introduction.—Nonlinear light-matter interaction plays a key role in manipulating light and matter at the nanoscale. In particular, the shift current, also known as the bulk photovoltaic effect (BPVE), is a second-order nonlinear optical (NLO) process that can directly convert light into electricity in crystals with broken inversion symmetry [1–3]. The BPVE has great advantages in many modern physical applications, e.g., new generation of solar cells [3–6], ultrasensitive optical detectors [7], and optically readable memristors and circuits [8]. Among these applications, the key step relies on the realization of giant and highly tunable NLO responses, which, however, is still a great challenge [5,8–15].

In the past years, great efforts have been made to understand the mechanism of BPVE and to find the ingredients for large-shift-current response [2,3,16–23]. Until now, although it is still an open question, some preliminary conclusions have been made; e.g., while the strength of the shift current may not depend on the intrinsic polarization of the system [3,16], it depends on the linear optical transition and shift-vector matrix elements [9–12,24,25]. Unfortunately, how to effectively tune the shift-vector matrix elements in a controllable way, which is key for tunable shift-current conductivity, is still largely unknown. Recently, several methods have been proposed to realize tunable shift currents, e.g., via the bulk piezophotovoltaic effect [26,27], flexophotovoltaic effect [28], and ferroicity engineering [10]; however, a continuous tunability in a very large photocurrent range is still unachievable.

In this Letter, based on a simple two-band model, we propose that an out-of-plane external electric field (E_{ext}) can continuously tune in-plane shift current along with its sign flip in a heteronodal-line (HNL) system. We name this effect the bulk electrophotovoltaic effect (BEPVE). The strong linear optical transition around the nodal loop may play a key role in generating giant shift current in a HNL system. Importantly, an E_{ext} can effectively control the radius of a nodal loop, which can continuously tune the shift-vector components inside and outside the nodal-loop with opposite signs. Using first-principles calculations (see Sec. I in Supplemental Material [29]), we discover that the van der Waals (vdW) heterobilayer $HSnN/MoS_2$ is a HNL system that can exhibit giant shift current around the nodal-loop region. Surprisingly, a relatively small E_{ext} enables a giant BEPVE with a continuous current change, which has been very difficult to realize in previously reported BPVE systems.

Concept of BEPVE.—Under electric field $E^b(\omega)$ at frequency ω and linearly polarized in the b direction, the shift-current density $\boldsymbol{J}$ is a second-order response, i.e., $J^a = \sigma^a_{bb}(\omega)E^b(\omega)E^b(-\omega)$, where a, b are Cartesian indices and the shift-current conductivity σ^a_{bb} [2] is given by

$$\sigma^a_{bb}(0;\omega,-\omega) = \frac{\pi e^3}{\hbar^2}\int \frac{d^3k}{8\pi^3}\sum_{nm} f_{nm}|r^b_{nm}|^2 R^{ab}_{nm}\delta(\omega_{mn}-\omega). \quad (1)$$

In Eq. (1), the r^b_{nm} is an optical-transition matrix element, which is related to the interband velocity matrix element

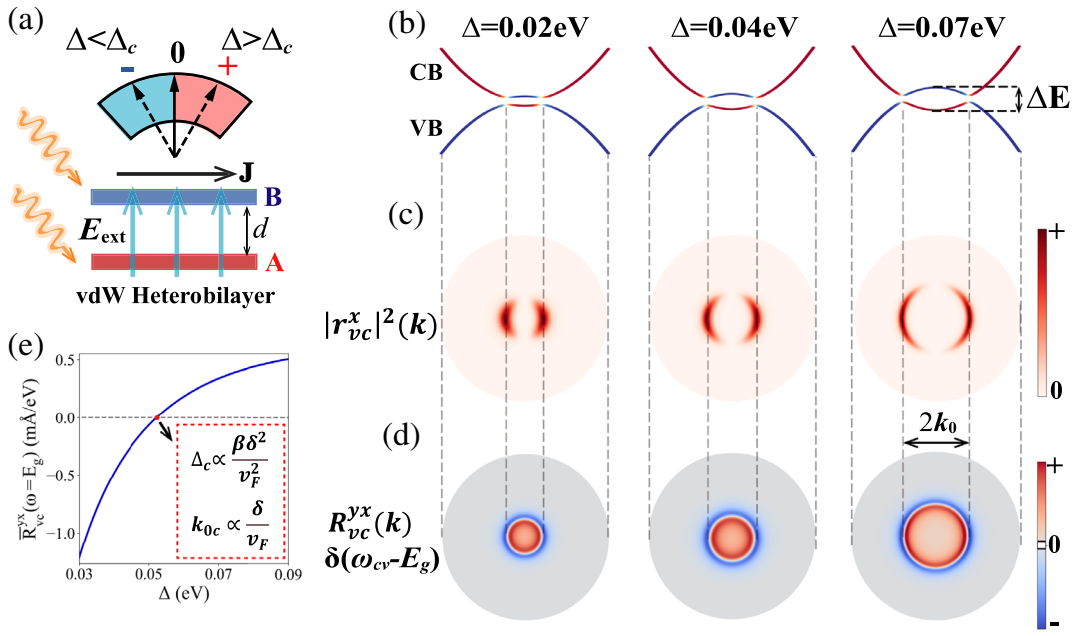

FIG. 1. (a) A vdW heterobilayer made of layer A and layer B under an out-of-plane E_{ext}. (b) Evolution of the band structures with the change of on-site-energy difference between two layers (Δ) in a HNL system. Δ can be effectively tuned by E_{ext}. Red (blue) band is contributed by layer A (B). ΔE measures the strength of the band crossing. k_0 is the radius of the nodal loop. (c) and (d) are the calculated k-resolved $|r^x_{vc}|^2$ and $R^{yx}_{vc}\delta(\omega_{cv}-E_g)$, two major components of σ^y_{xx} around the nodal loop, with different Δ, respectively. (e) Calculated $\bar{R}^{yx}_{vc}$ around the nodal loop as a function of Δ. Parameters of $\beta = 1$ eV/Å^2, $\delta = 0.01$ eV, $v_F = 0.02$ eV Å are adopted for the two-band model calculations.

v_{nm} via $r_{nm} = (v_{nm}/i\omega_{nm})(m \neq n)$. R^{ab}_{nm} is the shift vector that can be interpreted as the position change of a wave packet during its transition from the nth band to the mth band [2,16]. We can integrate R^{ab}_{mn} over the entire Brillouin zone (BZ) to obtain the aggregate shift vector $\bar{R}^{ab}$ [16], i.e., $\bar{R}^{ab}(\omega) = \Omega \int (d^3k/8\pi^3) \sum_{nm} f_{nm} R^{ab}_{nm} \delta(\omega_{mn} - \omega)$, where Ω is the volume of the unit cell. $\bar{R}^{ab}$ provides qualitative information about the strength and sign of the shift vector [16,24,25].

We consider a general 2×2 Hamiltonian to simulate the band structure of a HNL system:

$$H(k) = \sum_i \sigma_i f_i = \delta\sigma_x + v_F k_y \sigma_y + (\beta k^2 - \Delta)\sigma_z, \quad (2)$$

where $\sigma_i = \sigma_x, \sigma_y, \sigma_z$ are the Pauli matrices, δ is the interlayer coupling strength, and Δ is the on-site energy difference between the two layers. Without loss of generality, we take the linear term $v_F k_y$ to be in the y direction, which breaks the inversion symmetry and gives rise to the nonlinear shift current. The energies of the conduction band (CB) and valence band (VB) are given by $E_c = \epsilon$ and $E_v = -\epsilon$, respectively, and $\epsilon = (\sum_i f_i f_i)^{1/2}$. Subscripts v and c indicate the VB and CB, respectively. The radius of the nodal loop in momentum space is $k_0 = \sqrt{\Delta/\beta}$. On the nodal loop, the energy difference between E_c and E_v is

$$E_c - E_v = 2\sqrt{\delta^2 + v_F^2 k_y^2}, \quad (3)$$

and the band gap of the HNL system is $E_g = 2\delta$. v_F determines the anisotropy for the energy difference between the CB and VB on the nodal loop.

There are two independent nonvanishing components of R^{ab}_{vc} (i.e., R^{yx}_{vc} and R^{yy}_{vc}) in the HNL system described by Eq. (2). Based on the formula derivation (Sec. II in Supplemental Material [29]), R^{yx}_{vc} can be given as

$$R^{yx}_{vc} = \frac{1}{\frac{\delta}{v_F} + \frac{v_F}{\delta} k_y^2} \frac{\Delta - \beta k^2}{\sqrt{(\beta k^2 - \Delta)^2 + \delta^2 + v_F^2 k_y^2}}. \quad (4)$$

The expression of R^{yy}_{vc} is complex (Sec. II in Supplemental Material [29]).

For the vdW HNL system [Fig. 1(a)], its band structures under different Δ are shown in Fig. 1(b). Obviously, the larger the Δ, the larger the band crossing ΔE ($\Delta E = 2\sqrt{\Delta^2 + \delta^2}$). It is interesting to explore the $|r^x_{vc}|^2$ and $R^{yx}_{vc}\delta(\omega_{cv} - E_g)$, two key ingredients of σ^y_{xx} around the nodal loop, as a function of Δ. As shown in Fig. 1(c), the calculated $|r^x_{vc}|^2$ is mainly concentrated around the nodal-loop region, consistent with the fact that v_{nm} (ω_{nm}) has the maximum (minimum) value around the nodal loop (Fig. S2 in Supplemental Material [29]). Meanwhile, compared to a nodal-point (NP) system, the 2D HNL can generate much

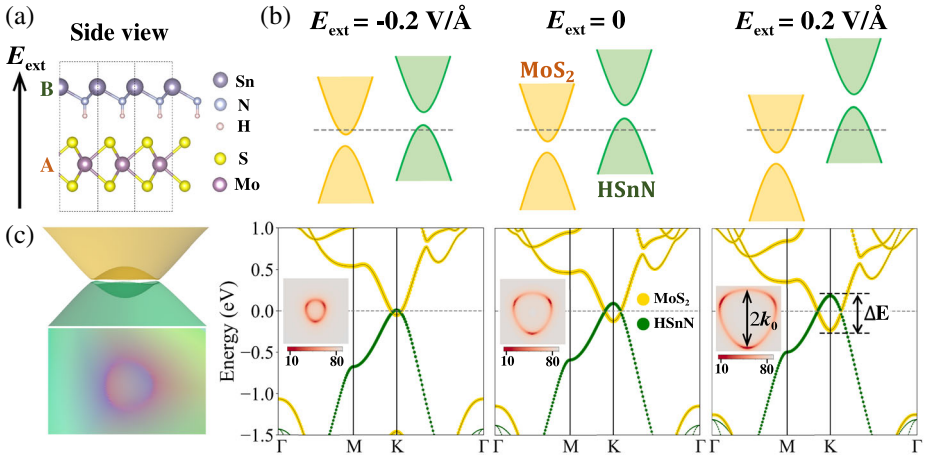

FIG. 2. (a) Side view of vdW heterobilayer HSnN/MoS_2. Unit cells are marked as dashed lines. (b) Schematic illustration (top figures) and projected band structures (bottom figures) of HSnN/MoS_2 under E_{ext}, in which the direction of E_{ext} is marked in (a). Insets of (b): nonuniform anticrossing band gaps on the nodal loop (unit: meV). (c) Side (top figures) and top (bottom figures) views of the 3D band structure of HSnN/MoS_2 around HNL ($E_{ext} = 0$ V/Å). Fermi level is set to zero.

stronger joint density of states (JDOS) $[\int \delta(\omega_{cv} - E_g)]$ around the nodal loop, which increases as k_0 increases [39,40]. Therefore, the ultralarge linear optical transition $[\int |r^x_{vc}|^2 \delta(\omega_{cv} - E_g)]$ may potentially induce a giant σ^y_{xx} around the nodal loop.

In a HNL system, $\bar{R}_{vc}$ can be well separated into two parts, i.e., $\bar{R}_{vc} = \bar{R}^{A\to B}_{vc} + \bar{R}^{B\to A}_{vc}$, in which $\bar{R}^{A\to B}_{vc}$ and $\bar{R}^{B\to A}_{vc}$ are contributed by the optical transition inside the nodal loop ($k < k_0$) and outside the nodal loop ($k > k_0$), respectively. As indicated in Eq. (4), $R^{yx}_{vc}(k) = 0$ on the nodal loop ($k = k_0$); the signs of $R^{A\to B}_{vc}$ and $R^{B\to A}_{vc}$ for the R^{yx}_{vc} component are always opposite. As shown in Fig. 1(d), by tuning Δ (k_0), it is possible to smoothly tune the values of $R^{A\to B}_{vc}\delta(\omega_{cv} - E_g)$ and $R^{B\to A}_{vc}\delta(\omega_{cv} - E_g)$, realizing the smooth change of $\bar{R}^{yx}_{vc}$ around the nodal-loop region. However, this sign flip across the nodal loop will not happen for R^{yy}_{vc} (Fig. S3 in Supplemental Material [29]). Figure 1(e) shows the calculated $\bar{R}^{yx}_{vc}$ as a function of Δ. Indeed, with the increase of Δ, $\bar{R}^{yx}_{vc}$ will gradually change and eventually flip its sign at a critical Δ (Δ_c) or critical k_0 (k_{0c}). Based on the formula derivation with some approximations (Sec. II in the Supplemental Material [29]), we can estimate Δ_c and k_{0c} as

$$\Delta_c \propto \frac{\beta\delta^2}{v_F^2}, \qquad k_{0c} \propto \frac{\delta}{v_F}. \tag{5}$$

Interestingly, k_{0c} and Δ_c are strongly related to the δ, β, and v_F values, which are variable in different HNL materials. In practice, Δ can be effectively tuned by the external E_{ext}. Based on this idea, we can propose a concept of an electric-field-tunable shift vector in a HNL system, as illustrated in Fig. 1(a), named BEPVE.

HNL in HSnN/MoS_2.—Both monolayer MX_2 (M = Mo, W; X = S, Se) and $ASnX$ (A = Na, H; $X = N$, P) have noticeable NLO responses [10,12,41–45]. Here we focus on the vdW heterobilayer formed by MoS_2 and HSnN. The HSnN is both dynamically and thermodynamically stable (Fig. S4 in the Supplemental Material [29]). The ground-state configuration is AB stacking with a $P3m1$ space group [Fig. 2(a) and Supplemental Material Fig. S5 [29]]. Figure 2(b) shows the band structures of HSnN/MoS_2. The bottom of the CB in MoS_2 is contributed by a Mo $3d_{z^2}$ orbital, while the top of the VB in HSnN is contributed by a Sn $5p_z$ orbital (Fig. S6 in the Supplemental Material [29]). When $E_{ext} = 0$ V/Å, these two band-edge states can cross each other, resulting in $\Delta E = 0.21$ eV. As shown in Fig. 2(c), the 3D band structure indicates that a HNL is formed in the entire BZ around Fermi level. The nodal loop exhibits a C_{3v}-like symmetry. Interestingly, the orbital hybridization between Mo $3d_{z^2}$ and Sn $5p_z$ can induce a small anticrossing band gap, which is nonuniform and in the range of 10–80 meV on the nodal loop [inset, Fig. 2(b)]. The band structure around the Fermi level has small changes under hybrid-functional calculations or with the inclusion of the spin-orbital-coupling (SOC) effect (Fig. S7 in the Supplemental Material [29]).

As shown in Fig. 1(b), an out-of-plane E_{ext} can adjust the ΔE between MoS_2 and HSnN. Indeed, as shown in Fig. 2(b), a positive (negative) E_{ext} can upshift (downshift) the energy level of HSnN with respect to MoS_2, increasing (decreasing) ΔE. Although the shape of the nodal loop is not circular, we can approximately estimate k_0 in Fig. 2(b). With E_{ext} gradually increasing from −0.2 to 0.2 V/Å, k_0 can increase from to 0.41 $Å^{-1}$. Overall, HSnN/MoS_2 is a good HNL system with a tunable nodal loop.

Giant BEPVE around a nodal loop. —Based on the symmetry restriction, there is only one (four) independent nonvanishing σ components in monolayer MoS_2 (HSnN). We focus on the in-plane σ^y_{xx} ($\sigma^y_{xx} = \sigma^x_{xy} = -\sigma^y_{yy}$) component. The calculated σ^y_{xx} spectra of monolayer MoS_2

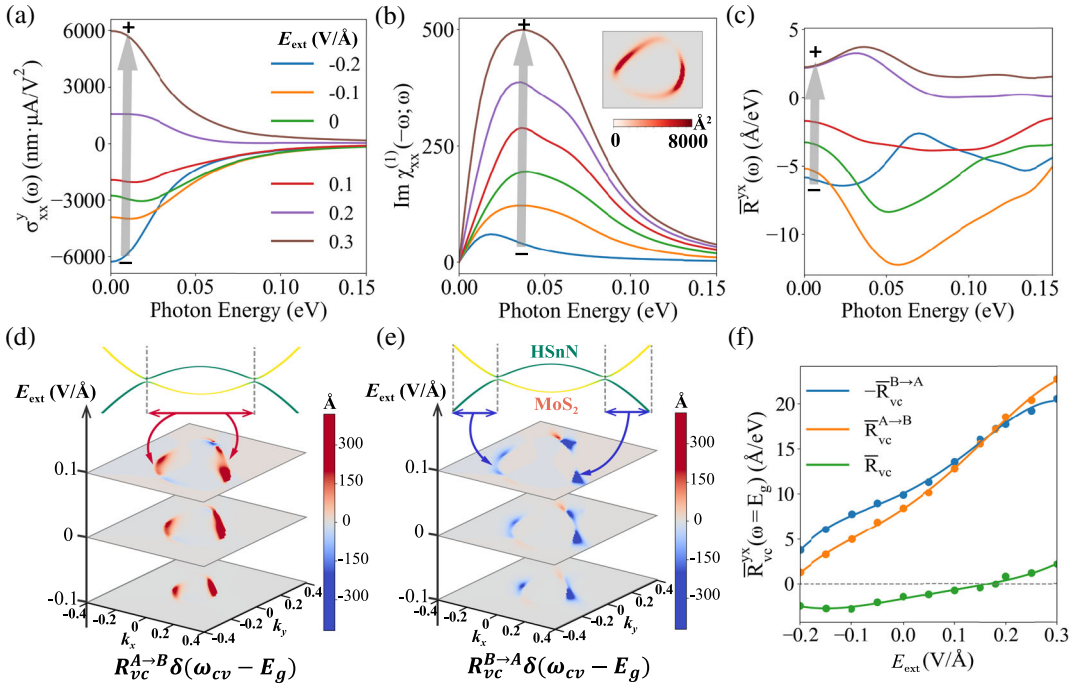

FIG. 3. (a) Shift-current conductivities σ_{xx}^{y}, (b) linear absorption spectra $\mathrm{Im}\chi_{xx}^{(1)}$, and (c) aggregate shift vectors $\bar{R}^{yx}$ in HSnN/MoS_2 as a function of the photon energy under different E_{ext}. Inset of (b): k-resolved $|r_{vc}^{x}|^2$ between two HNL bands. (d) and (e) are k-resolved $R_{vc}^{A\to B}\delta(\omega_{cv}-E_g)$ and $R_{vc}^{B\to A}\delta(\omega_{cv}-E_g)$ between these two HNL bands around the nodal loop, respectively. (f) $\bar{R}_{vc}^{A\to B}$, $\bar{R}_{vc}^{B\to A}$, and $\bar{R}_{vc}^{yx}$ between two HNL bands around the nodal loop as a function of E_{ext}. A(B) → B(A) means MoS_2(HSnN) → HSnN(MoS_2).

and HSnN are shown in Fig. S8 in the Supplemental Material [29], and their peak values are located at >2 eV. Interestingly, as shown in Fig. 3(a), when the heterobilayer is formed, besides the same peak spectra at high photon energy as individual monolayers, a new peak emerges around the nodal loop, which decreases gradually as the photon energy increases. This new peak value is as huge as $\sim -3000\ \mathrm{nm\,\mu A/V^2}$.

Next, we consider the E_{ext} effect. It is not surprising that σ_{xx}^{y} of both MoS_2 and HSnN is insensitive to E_{ext} (Fig. S9 in the Supplemental Material [29]). After forming the HNL, σ_{xx}^{y} of HSnN/MoS_2 strongly varies with E_{ext}. As shown in Figs. 3(a) and S10(a) in the Supplemental Material [29], when E_{ext} gradually changes from −0.2 to ∼0.18 V/Å, the peak around the nodal-loop region gradually decreases from ~ -6280 to $\sim 0\ \mathrm{nm\,\mu A/V^2}$. When E_{ext} further increases from ∼0.18 to 0.3 V/Å, the peak gradually increases from ∼0 to $\sim 6000\ \mathrm{nm\,\mu A/V^2}$, along with the sign flip. This conclusion does not change when the SOC effect is included [Fig. S10(b) in the Supplemental Material [29]]. Clearly, the formation of the HNL plays a key role in forming (i) a huge σ_{xx}^{y} peak and (ii) an E_{ext}-tunable σ_{xx}^{y} peak around nodal-loop region.

It is interesting to further explore the origin of (i)–(ii). As shown in Fig. 3(b), the ultrastrong linear optical absorption spectrum ($\mathrm{Im}\chi_{xx}^{(1)}$) originating from the large $|r_{vc}^{x}|^2$ [inset of Fig. 3(b)] and HNL-induced large JDOS could be the key to generating a huge σ_{xx}^{y}. When $E_{\mathrm{ext}}=0$ V/Å, the $\mathrm{Im}\chi_{xx}^{(1)}$ is peaked around the nodal loop with a large value of ∼195, which is ∼22 (∼18) times larger than that of monolayer HSnN (MoS_2) (Fig. S4 in the Supplemental Material [29]). The k-resolved $|r_{vc}^{x}|^2$ is always concentrated around the nodal loop under different E_{ext} (Fig. S11 in the Supplemental Material [29]), agreeing with Fig. 1(c). When E_{ext} gradually changes from −0.2 to 0.3 V/Å, the increased band inversion can gradually increase k_0, giving rise to the increased $\mathrm{Im}\chi_{xx}^{(1)}$. Usually, the stronger the $\mathrm{Im}\chi_{xx}^{(1)}$, the larger the NLO response [3,9,17]. Surprisingly, our case does not follow this common rule, indicating the unusual role of the shift vector. Indeed, as shown in Fig. 3(c), the trend of $\bar{R}^{yx}$, including its sign, around the nodal-loop region matches the trend of σ_{xx}^{y} under different E_{ext}.

We have further calculated the k-resolved $R_{vc}^{yx}\delta(\omega_{cv}-E_g)$ between these two HNL bands. R_{vc} can be projected into two parts, i.e., $R_{vc}^{A\to B}$ and $R_{vc}^{B\to A}$. As shown in Fig. 3(d) [Fig. 3(e)], the $R_{vc}^{A\to B}\delta(\omega_{cv}-E_g)[R_{vc}^{B\to A}\delta(\omega_{cv}-E_g)]$ represents the shift vector contributed by the optical transition from MoS_2 (HSnN) to HSnN (MoS_2) around the nodal loop, which is concentrated inside (outside) the nodal loop in the k space, agreeing with Fig. 1(d). On the nodal loop, R_{vc}^{yx} is zero. With E_{ext} changing from negative to positive, k_0 of the nodal loop increases, which can further manipulate the k-space distribution of $R_{vc}^{A\to B}\delta(\omega_{cv}-E_g)$ and $R_{vc}^{B\to A}\delta(\omega_{cv}-E_g)$. σ_{xx}^{y} resembles a similar k-space distribution to $R_{vc}^{yx}\delta(\omega_{cv}-E_g)$ (Fig. S11 in the Supplemental

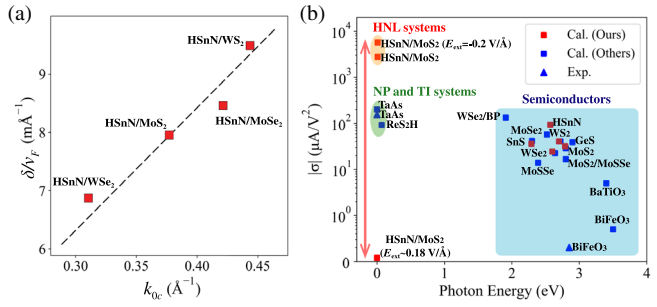

FIG. 4. (a) Relation between calculated δ/v_F and k_{0c} in four HSnN/MX_2 (M = Mo, W; X = S, Se) systems exhibiting a nearly linear dependence. (b) Comparison of $|\sigma|$ between heterobilayer HSnN/MoS_2 and other widely studied BPVE materials in the literature [7,9–11,13,16,46–48].

Material [29]). The calculated $\bar{R}_{vc}^{A\to B}$ and $\bar{R}_{vc}^{B\to A}$ are shown in Fig. 3(f), exhibiting two major features: (1) the signs of $\bar{R}_{vc}^{A\to B}$ and $\bar{R}_{vc}^{B\to A}$ are always opposite, and (2) the slope of $|\bar{R}_{vc}^{A\to B}|$ is larger than that of $|\bar{R}_{vc}^{B\to A}|$ under $E_{\rm ext}$. Therefore, $\bar{R}_{vc}^{yx} = \bar{R}_{vc}^{A\to B} + \bar{R}_{vc}^{B\to A}$ can be gradually changed as a function of $E_{\rm ext}$. Interestingly, the sign of $\bar{R}_{vc}^{yx}$ is enforced to flip at a critical $E_{\rm ext}$ of ~0.18 V/Å, so as to σ_{xx}^{y} [Fig. S10(a) in the Supplemental Material [29]]. Now, we can conclude that while the strong $\mathrm{Im}\chi_{xx}^{(1)}$ can generate a giant σ_{xx}^{y} peak around the nodal loop, the nodal-loop-dependent $\bar{R}_{vc}^{yx}$ plays a key role in manipulating this σ_{xx}^{y} peak, eventually realizing a giant BEPVE.

It is interesting to further understand the sign flip of $\bar{R}_{vc}^{yx}$ (σ_{xx}^{y}). We further calculate the other three HSnN/MX_2 (M = Mo, W; X = S, Se) materials. First, following a similar calculation procedure for HSnN/MoS_2, we can determine the critical $E_{\rm ext}$ for sign flip of σ_{xx}^{y} in different HSnN/MX_2 (Fig. S12 in the Supplemental Material [29]). Second, based on Eq. (3), the values of δ, v_F, and k_{0c} in these materials are further estimated in the electronic structures under their critical $E_{\rm ext}$ (Table S1 in the Supplemental Material [29]). Finally, as shown in Fig. 4(a), k_{0c} is almost linearly dependent on δ/v_F in these four systems, agreeing well with Eq. (5). The small deviation may be due to the approximation on estimating k_{0c} in HSnN/MX_2 [Fig. 2(b)].

Discussion.—It is interesting to compare σ of HSnN/MoS_2 with other widely studied BPVE materials. As shown in Fig. 4(b), we have collected the peak values in the largest σ component around the band gap in a couple of 2D and 3D BPVE systems reported in the literature [7,9–11,13,16,46–48]. Among these materials, we have recalculated four of them (Fig. S13 in the Supplemental Material [29]), i.e., MoS_2, SnS, WS_2, and WSe_2, using similar computational parameters as in the literature [10], which produce similar results. Interestingly, these BPVE materials in Fig. 4(b) can be roughly divided into three categories: (i) common semiconductors with a sizable band gap, e.g., $|\sigma_{xx}^{z}| \sim 5\ \mu\mathrm{A/V^2}$ for $BaTiO_3$ [16] and $|\sigma_{yy}^{y}| \sim 40\ \mu\mathrm{A/V^2}$ for monolayer MoS_2 [10]; (ii) NP and topological insulator systems with a tiny band gap, e.g., $|\sigma_{xz}^{x}| \sim 200\ \mu\mathrm{A/V^2}$ for TaAs [7,46,49] and $|\sigma_{yy}^{y}| \sim 90\ \mu\mathrm{A/V^2}$ for ReS_2H [9]; (iii) our proposed HNL system with a tiny band gap, e.g., $|\sigma_{yy}^{y}| \sim 2800$ and $\sim 6200\ \mu\mathrm{A/V^2}$ for HSnN/MoS_2 under an $E_{\rm ext}$ of 0 and -0.2 V/Å, respectively. Overall, the $|\sigma|$ of category (iii) is 1 (2) order of magnitude larger than that of category (ii) [(i)], indicating that the HNL system is suitable to generate a giant $|\sigma|$. Most importantly, besides of the sign flip, the $|\sigma_{xx}^{y}|$ value of HSnN/MoS_2 can be hugely and continuously tuned from 0 to $\sim 6200\ \mu\mathrm{A/V^2}$ under relatively small $E_{\rm ext}$, induced by the concept of BEPVE.

We thank Dr. Haowei Chen at Tsinghua University for helpful discussions. This work is supported by NSFC (Grants No. 12088101 and No. 12174404), the National Key Research and Development of China (Grant No. 2022YFA1402401), NSAF (Grant No. U2230402), and the Open Research Fund Program of the State Key Laboratory of Low-Dimensional Quantum Physics. Calculations were done in the Tianhe-JK cluster at CSRC.

*Bing.Huang@csrc.ac.cn

[1] R. von Baltz and W. Kraut, Phys. Rev. B **23**, 5590 (1981).
[2] J. E. Sipe and A. I. Shkrebtii, Phys. Rev. B **61**, 5337 (2000).
[3] L. Z. Tan, F. Zheng, S. M. Young, F. Wang, S. Liu, and A. M. Rappe, npj Comput. Mater. **2**, 16026 (2016).
[4] Y. J. Zhang, T. Ideue, M. Onga, F. Qin, R. Suzuki, A. Zak, R. Tenne, J. H. Smet, and Y. Iwasa, Nature (London) **570**, 349 (2019).
[5] Y. Li, J. Fu, X. Mao, C. Chen, H. Liu, M. Gong, and H. Zeng, Nat. Commun. **12**, 5896 (2021).
[6] I. Grinberg, D. V. West, M. Torres, G. Gou, D. M. Stein, L. Wu, G. Chen, E. M. Gallo, A. R. Akbashev, P. K. Davies *et al.*, Nature (London) **503**, 509 (2013).
[7] G. B. Osterhoudt, L. K. Diebel, M. J. Gray, X. Yang, J. Stanco, X. Huang, B. Shen, N. Ni, P. J. W. Moll, Y. Ran *et al.*, Nat. Mater. **18**, 471 (2019).
[8] Z. Xiao, Y. Yuan, Y. Shao, Q. Wang, Q. Dong, C. Bi, P. Sharma, A. Gruverman, and J. Huang, Nat. Mater. **14**, 193 (2015).
[9] C. Zhang, H. Pi, L. Zhou, S. Li, J. Zhou, A. Du, and H. Weng, Phys. Rev. B **105**, 245108 (2022).
[10] H. Wang and X. Qian, Sci. Adv. **5**, eaav9743 (2019).
[11] A. Strasser, H. Wang, and X. Qian, Nano Lett. **22**, 4145 (2022).
[12] A. M. Schankler, L. Gao, and A. M. Rappe, J. Phys. Chem. Lett. **12**, 1244 (2021).
[13] S. M. Young, F. Zheng, and A. M. Rappe, Phys. Rev. Lett. **109**, 236601 (2012).
[14] K. Yao, N. R. Finney, J. Zhang, S. L. Moore, L. Xian, N. Tancogne-Dejean, F. Liu, J. Ardelean, X. Xu, D. Halbertal *et al.*, Sci. Adv. **7**, eabe8691 (2021).
[15] S. Yuan, Y. Wu, Z. Dang, C. Zeng, X. Qi, G. Guo, X. Ren, and J. Xia, Phys. Rev. Lett. **127**, 153901 (2021).

[16] S. M. Young and A. M. Rappe, Phys. Rev. Lett. **109**, 116601 (2012).
[17] A. M. Cook, M. F. B, F. de Juan, S. Coh, and J. E. Moore, Nat. Commun. **8**, 14176 (2017).
[18] J. Ahn, G.-Y. Guo, and N. Nagaosa, Phys. Rev. X **10**, 041041 (2020).
[19] B. M. Fregoso, T. Morimoto, and J. E. Moore, Phys. Rev. B **96**, 075421 (2017).
[20] L. K. Shi, D. Zhang, K. Chang, and J. C. W. Song, Phys. Rev. Lett. **126**, 197402 (2021).
[21] D. E. Parker, T. Morimoto, J. Orenstein, and J. E. Moore, Phys. Rev. B **99**, 045121 (2019).
[22] T. Holder, D. Kaplan, and B. Yan, Phys. Rev. Res. **2**, 033100 (2020).
[23] D. Kaplan, T. Holder, and B. Yan, arXiv:2208.00827.
[24] T. Rangel, B. M. Fregoso, B. S. Mendoza, T. Morimoto, J. E. Moore, and J. B. Neaton, Phys. Rev. Lett. **119**, 067402 (2017).
[25] B. Kim, N. Park, and J. Kim, Nat. Commun. **13**, 3237 (2022).
[26] S. Nadupalli, J. Kreisel, and T. Granzow, Sci. Adv. **5**, eaau9199 (2019).
[27] Y. Dong, M. M. Yang, M. Yoshii, S. Matsuoka, S. Kitamura, T. Hasegawa, N. Ogawa, T. Morimoto, T. Ideue, and Y. Iwasa, Nat. Nanotechnol. **18**, 36 (2023).
[28] J. Jiang, Z. Chen, Y. Hu, Y. Xiang, L. Zhang, Y. Wang, G. C. Wang, and J. Shi, Nat. Nanotechnol. **16**, 894 (2021).
[29] See Supplemental Material at http://link.aps.org/supplemental/10.1103/PhysRevLett.130.256902 for details about the computational methods, formula derivation and parameter tests, stacking configurations, band structures, linear absorption spectra, and shift-current spectra calculations for different systems, which includes Refs. [30–38].
[30] G. Kresse and J. Furthmüller, Phys. Rev. B **54**, 11169 (1996).
[31] P. E. Blöchl, Phys. Rev. B **50**, 17953 (1994).
[32] J. P. Perdew, K. Burke, and M. Ernzerhof, Phys. Rev. Lett. **77**, 3865 (1996).
[33] A. A. Mostofi, J. R. Yates, Y.-S. Lee, I. Souza, D. Vanderbilt, and N. Marzari, Comput. Phys. Commun. **178**, 685 (2008).
[34] N. Marzari, A. A. Mostofi, J. R. Yates, I. Souza, and D. Vanderbilt, Rev. Mod. Phys. **84**, 1419 (2012).
[35] P. Li, X. Jiang, M. Huang, L. Kang, S. Chen, A. Gali, and B. Huang, Cell Rep. Phys. Sci. **3**, 101111 (2022).
[36] W. Tan, X. Jiang, Y. Li, X. Wu, J. Wang, and B. Huang, Adv. Funct. Mater. **32**, 2208023 (2022).
[37] X. Jiang, L. Ye, X. Wu, L. Kang, and B. Huang, Phys. Rev. B **106**, 195126 (2022).
[38] J.-M. Lihm and C.-H. Park, Phys. Rev. X **11**, 041053 (2021).
[39] J. Wang, X. Sui, W. Duan, F. Liu, and B. Huang, Proc. Natl. Acad. Sci. U.S.A. **118**, e2023029118 (2021).
[40] J. Wang, Y. Liu, K.-H. Jin, X. Sui, L. Zhang, W. Duan, F. Liu, and B. Huang, Phys. Rev. B **98**, 201112(R) (2018).
[41] H. Wang and X. Qian, Nano Lett. **17**, 5027 (2017).
[42] S. Zhang, L. Kang, and Z. Lin, Nanoscale **12**, 14895 (2020).
[43] X. Jiang, L. Kang, and B. Huang, Phys. Rev. B **105**, 045415 (2022).
[44] L. M. Malard, T. V. Alencar, A. P. M. Barboza, K. F. Mak, and A. M. de Paula, Phys. Rev. B **87**, 201401(R) (2013).
[45] X. Yin, Z. Ye, D. A. Chenet, Y. Ye, K. O'Brien, J. C. Hone, and X. Zhang, Science **344**, 488 (2014).
[46] Q. Ma, S.-Y. Xu, C.-K. Chan, C.-L. Zhang, G. Chang, Y. Lin, W. Xie, T. Palacios, H. Lin, S. Jia *et al.*, Nat. Phys. **13**, 842 (2017).
[47] W. Ji, K. Yao, and Y. C. Liang, Phys. Rev. B **84**, 094115 (2011).
[48] T. Akamatsu, T. Ideue, L. Zhou, Y. Dong, S. Kitamura, M. Yoshii, D. Yang, M. Onga, Y. Nakagawa, K. Watanabe *et al.*, Science **372**, 68 (2021).
[49] L. Wu, S. Patankar, T. Morimoto, N. L. Nair, E. Thewalt, A. Little, J. G. Analytis, J. E. Moore, and J. Orenstein, Nat. Phys. **13**, 350 (2017).